2007 IEEE International Conference on
Robotics and Automation
Roma, Italy, 10-14 April 2007

A Strategy for Vision-Based Controlled Pushing of Microparticles

Nicholas A. Lynch, Cagdas Onal, Eugenio Schuster, and Metin Sitti

Abstract— **In this paper, a strategy for controlled pushing is presented for microassembly of 4.5 µm polystyrene particles on a flat glass substrate using an atomic force microscope probe tip. Real-time vision based feedback from a CCD camera mounted to a high resolution optical microscope is used to track particle positions relative to the tip and target position. Tip-particle system is modeled in 2D as a non-holonomic differential drive robot. Effectiveness of the controller is demonstrated through experiments performed using a single goal position as well as linking a series of target positions to form a single complex trajectory. Cell decomposition and wavefront expansion algorithms are implemented to autonomously locate a navigable path to a specified target position. Control strategy alleviates problem of slipping and spinning during pushing.**

I. Introduction

MANIPULATION and assembly at the microscale and nanoscale has been an area of considerable research over the past several years. The overall goal is to form specific functional materials, devices, and systems through the positioning of individual micro/nanoscale materials. The results of this research have a wide range of applications stretching from MEMS and computer data storage to biotechnology and materials fabrication.

Critical to the development of microassmebly is the study of the basic modes of manipulation such as pushing, pulling, and pick and place. The primary tool used for manipulation is the atomic force microscope (AFM). The AFM is a subclass of the scanning probe microscope family featuring a sharp tip mounted to a microcantilever and is typically used as an imaging tool. During an AFM scan the deflections of the microcantilever due to changes in the surface topology are recorded and assembled to form an image of the sample. As a manipulation tool, the AFM probe tip can be used to directly contact and position individual particles.

Prior research has demonstrated the ability to position individual particles through both pushing and pulling with sub-micrometer precision [1]-[6]. In each of these experiments, nanoparticles or microparticles are deposited onto a glass slide mounted below the AFM tip. The dynamic mode, rolling, sliding or slip-stick, is a function of the size of the particle, the radius of the probe tip, the force applied to the particle, and the tip-particle contact angle [7]. Particle positioning through pulling has been only achieved by selecting these parameters such that the adhesion force at the tip-particle interface exceeds the forces at the particle-substrate interface. However for most cases, adhesion forces at the particle-substrate interface are such that pulling cannot be achieved.

The general approach for past manipulation trials has been to define a formation for the particle, automatically or manually match each particle to a specific position, and then either push or pull particles one by one to their specified position. In moving each particle to their goal position the path consists of either a straight line or a series of connected straight lines regardless or whether pushing or pulling is used. Strong results have been achieved using pulling to position the particles [1]. However, as stated above, pulling is only a viable option for specific tip-particle combinations. Success has also been achieved through pushing, yet a common problem is that the particle will slip or spin about the tip [2], [5]. In these cases the program must be stopped and the tip repositioned behind the particle, significantly slowing down the manipulation procedure.

In this work an approach to controlled pushing at the microscale is presented. The primary motivation for this work is the need to eliminate sliding and spinning around the tip during manipulation. Pushing is the desired mode of manipulation as pulling can only be achieved for larger particles where larger adhesion forces are possible due to the large surface contact area at the tip-particle interface. As manipulations techniques are scaled down to the nanoscale only manipulation through pushing will be possible. It is with this in mind that the strategies presented in this paper focus upon controlled pushing.

The organization to this paper is as follows. In Section II the manipulation problem is presented along with a description of the experimental setup. This includes an overview of the model of the tip-particle interface, the critical assumptions, and a derivation of the kinematic model for the particle. In Section III the derivation of the controller is presented along with a discussion of its stability properties. In Section IV the controller is implemented on the physical system and the results from a series of manipulation experiments is presented. Finally, the paper is concluded in Section V with a summary of results and a discussion of future work.

Manuscript received January 31, 2007. This work was supported in part by a grant from the Commonwealth of Pennsylvania, Department of Community and Economic Development, through the Pennsylvania Infrastructure Technology Alliance (PITA), and partially by the NSF CAREER award program (IIS-0448042).

N. Lynch and E. Schuster are respectively with the Department of Electrical Engineering and the Department of Mechanical Engineering and Mechanics at Lehigh University, Bethlehem, PA 18015, USA (nal4@lehigh.edu, schuster@lehigh.edu).

C. Onal and M. Sitti are with the Department of Mechanical Engineering at Carnegie Mellon University, Pittsburgh, PA 15213, USA (cagdas@cmu.edu, sitti@cmu.edu).

II. Problem Definition

A. Experimental Setup

The manipulation experiments presented in this paper were performed on the custom-built AFM setup in the NanoRobotics Laboratory at Carnegie Mellon University. This is the same setup used by [1], [2], and [5]. The custom AFM is built around a high resolution optical microscope (Nikon Eclipse L200) with up to 3000x magnification. Polystyrene (PS) particles of 4.5 μm diameter are deposited onto the bottom of a transparent glass slide. This glass side is mounted to a high precision XYZ piezoelectric stage. This stage has a range of 100 μm along the x and y axes with +/- 10 nm precision and a range of 15 μm along the z axis with +/- 2 nm precision. This stage receives position inputs from the host PC via D/A card and has its own feedback loop allowing quick response to control inputs. Mounted to a manual coarse positioning stage below the glass slide is a 20 nm radius AFM probe tip (ULTRASHARP NC from Micromash Inc.). To close the feedback loop, a CCD color video camera is mounted on the optical microscope. Connected to the host PC via a framegrabber card, this camera provides updates at approximately 10-15 Hz. Fig. 1 shows a simple diagram of the experimental setup.

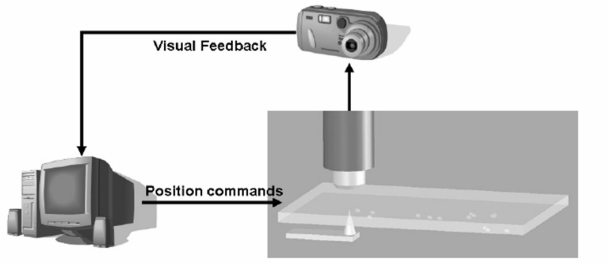

Fig. 1. Simple diagram of the experimental setup [1]

The first step in the manipulation program is locating each of the particles as well as the AFM tip in the image plane. Particles are detected by the gradient detection algorithm presented and implemented in [1], [8]. This approach searches the thresholded gradient image for opposing vector pairs in order to locate the spherical PS particles. Typically the Hough transform is utilized for the detection of circular shapes. However the Hough transform is often slow and difficult to implement in real-time image processing. Given the controlled environment of the manipulation trials and the known geometry of the PS particles, the gradient detection algorithm is an adequate solution for particle detection.

B. Tip-Particle Modeling

The first step of the design of the controller is modeling the tip-particle interaction and defining the particle kinematics. At the microscale and nanoscale adhesion forces dominate, therefore gravitational and inertial forces are neglected. The forces at the particle-substrate interface are a function of the contact area (A_s) and the normal force (F_s) at the tip-particle interface. The contact area can be found using the Johnson-Kendall-Roberts (JKR) model for contact mechanics,

$$A_s = \pi\left[\frac{R_{sp}}{K_{sp}}\left(F_s + 3\pi R_{sp}\omega_{sp} + \sqrt{6\pi R_{sp}\omega_{sp}F_s + \left(3\pi R_{sp}\omega_{sp}\right)^2}\right)\right]^{\frac{2}{3}}, \quad (1)$$

where K_{sp} is the equivalent modulus of elasticity of the substrate and the particle, ω_{sp} is the interaction free energy, and R_{sp} is the equivalent radius [9]. Using these parameters the condition for sliding with respect to the sliding force f_s is defined

$$f_s > \mu F_s + \tau A_s . \quad (2)$$

Note that μ is the friction coefficient and τ is the shear strength of the surface in contact for sliding.

Based upon the results presented in [7] for the selected particle size and tip radius, the predicted mode of behavior for the particle is sliding. Additionally, because these manipulation tasks are performed at relatively slow speeds, the system is assumed to be in quasi-static equilibrium and damping and inertial forces are neglected. Furthermore, because the tip used is relatively rigid and the radius tip is small relative to the radius of the particle, deflections of the tip during manipulation are neglected. Motion of the particle is restricted to the x-y plane. Therefore, the particle is modeled as having a translational velocity v_{trans} and a rotational velocity ω in the x-y plane. The motion of the particle is driven by the AFM probe tip which has velocity v_{tip}. The motion of the tip and particle is depicted in Fig. 2.

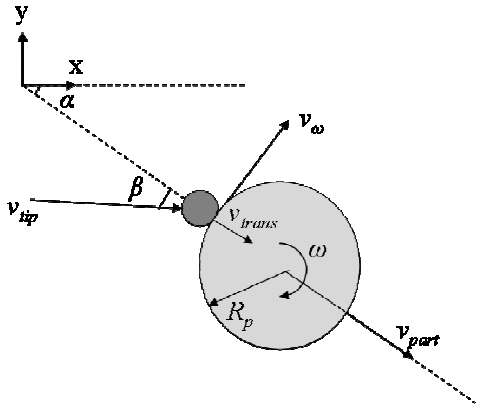

Fig. 2. Schematic of tip-particle interaction model

The input to the system is the tip velocity with magnitude v_{tip} and direction α-β which can be set by changing the magnitude of components $\dot{x}_{tip}$ and $\dot{y}_{tip}$. The tip imparts a velocity v_{trans} on the particle along with rotational velocity ω. The velocity vector is directed along the angle α which represents the orientation of the tip with respect to the particle. The relationship between the particle and the tip is given by

$$v_{trans} = v_{tip}\cos\beta , \quad (3)$$

$$\omega = \frac{v_\omega}{R_p} = \frac{v_{tip}}{R_p}\sin\beta , \beta \in \left[-\frac{\pi}{2}, \frac{\pi}{2}\right]. \quad (4)$$

Using the above equations, the model for the particle kinematics can be defined as

$$\begin{bmatrix} \dot{x} \\ \dot{y} \\ \dot{\alpha} \end{bmatrix}_{part} = \begin{bmatrix} \cos(\alpha) & 0 \\ \sin(\alpha) & 0 \\ 0 & -1 \end{bmatrix} \begin{bmatrix} v_{trans} \\ \omega \end{bmatrix}. \quad (5)$$

Using the kinematic model defined above, a controller is defined in the next section. The controller uses the components of the tip velocity vector v_{tip}, $\dot{x}_{tip}$ and $\dot{y}_{tip}$, to control the translational and rotational velocities of the particle. It should be noted that though the controller model is derived assuming that the tip moves to position particles, the tip actually remains stationary. As noted in the description of the experimental setup, the piezoelectric stage, to which the slide containing the deposited particles is mounted, is moved relative to the tip. Despite the discrepancy, the relative motion between the tip and the microparticles remains the same and only requires a sign change for implementation.

III. Controller Design

In Section II the kinematic equations (5) for the system were defined. In this section the controller to be used will be outlined along with a discussion of its stability properties. As discussed earlier, the goal is to design a controller that can drive a selected particle to a predefined target position with pushing as the only mode of motion. The model for the particle driven by the tip presented earlier mirrors a simple model for a non-holonomic differential drive vehicle. Feedback control and motion planning for non-holonomic vehicles has been an area of considerable study in the past [10]-[12]. Therefore, given the similarity of the kinematics models, many of the control strategies and algorithms in the macro world can be scaled down for use in micromanipulation and nanomanipulation.

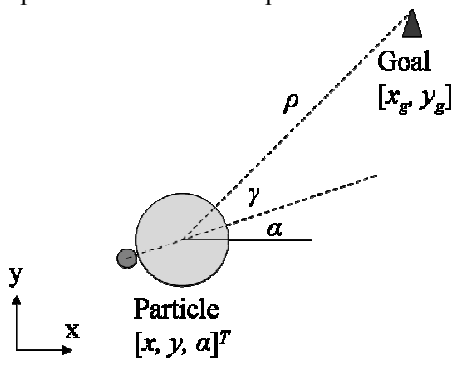

Fig. 3. Schematic of controller model variables

Consider the situation shown in Fig. 3. A PS particle is located in a given plane with initial position $[x, y, \alpha]^T$. Note that the orientation of the tip-particle system is defined by the position of the tip relative to the center of the particle. A goal position, $[x_g, y_g]^T$, is predefined. The goal of the controller is to drive the particle to the goal position by controlling the velocity, v_{trans}, and the rotation ω. The kinematic model in (5) can be transformed to polar coordinates by

$$\rho = \sqrt{(x_g - x)^2 + (y_g - y)^2}, \quad (6)$$

$$\gamma = -\alpha + \arctan\left(\frac{(y_g - y)}{(x_g - x)}\right). \quad (7)$$

Applying the above equations to (5) results in the polar system

$$\begin{bmatrix} \dot{\rho} \\ \dot{\gamma} \end{bmatrix}_{part} = \begin{bmatrix} -\cos\gamma & 0 \\ \dfrac{\sin\gamma}{\rho} & 1 \end{bmatrix} \begin{bmatrix} v_{trans} \\ \omega \end{bmatrix}. \quad (8)$$

The next step is the design of the control signals $v_{trans}(t)$ and $\omega(t)$. With this purpose we define the proportional control laws,

$$v_{trans} = k_\rho \rho, \ \omega = -k_\gamma \gamma, \quad (9)$$

where $k_\rho > 0$ and $k_\gamma > 0$ are positive constant gains.

Theorem: The control law (9), with $k_\gamma > k_\rho\left(1 + \bar{\rho}^2/2\right)$ makes the origin of system (8) asymptotically stable within the region of attraction defined by $\rho \in [0, \bar{\rho}]$ and $\gamma \in [-\pi, \pi]$, with $\bar{\rho} > 0$ arbitrary.

Proof: Substituting the control law into the kinematic model (8) results in the closed-loop system described by

$$\begin{bmatrix} \dot{\rho} \\ \dot{\gamma} \end{bmatrix}_{part} = \begin{bmatrix} -k_\rho \rho \cos\gamma \\ k_\rho \sin\gamma - k_\gamma \gamma \end{bmatrix}. \quad (10)$$

We define the Lyapunov function candidate

$$V = \frac{1}{2}\rho^2 + \frac{1}{2}\gamma^2. \quad (11)$$

The system is asymptotically stable [14] if it can be established that $\dot{V}(\rho, \gamma) < 0 \ \ \forall (\rho, \gamma) \neq (0,0)$ within the region of attraction. Differentiating V with respect to time yields

$$\dot{V} = \rho\dot{\rho} + \gamma\dot{\gamma}. \quad (12)$$

Substituting the equations given in (10) into (12) yields

$$\dot{V} = -k_\rho \rho^2 \cos\gamma + k_\rho \gamma \sin\gamma - k_\gamma \gamma^2. \quad (13)$$

Since $0 \leq \sin\gamma/\gamma \leq 1 \Rightarrow \gamma\sin\gamma \leq \gamma^2$ ($\gamma \in [-\pi, \pi]$), we can write

$$\dot{V} \leq -k_\rho \rho^2 \cos\gamma - \left(k_\gamma - k_\rho\right)\gamma^2 \quad (14)$$

The derivative w.r.t. γ of the right hand side of (14) yields

$$-2\left(k_\gamma - k_\rho\right)\gamma\left[1 - \frac{k_\rho \rho^2}{2\left(k_\gamma - k_\rho\right)}\frac{\sin\gamma}{\gamma}\right]. \quad (15)$$

We can note that this term will be zero only for $\gamma = 0$ since $0 \leq \sin\gamma/\gamma \leq 1$ and $k_\gamma > k_\rho\left(1 + \bar{\rho}^2/2\right)$ implies that $k_\rho \rho^2 / 2\left(k_\gamma - k_\rho\right) \leq k_\rho \bar{\rho}^2 / 2\left(k_\gamma - k_\rho\right) < 1$.

Therefore, the right hand side of (14) has a critical point (maximum) at $\gamma = 0$ for each ρ, equal to $-k_\rho \rho^2 \leq 0$,

which implies that $\dot{V} < 0 \ \ \forall(\rho,\gamma) \neq (0,0)$ within the region of attraction. Therefore, the origin of system (10) is asymptotically stable.

The condition $k_\gamma > k_\rho\left(1+\bar{\rho}^2/2\right)$ is sufficient but not necessary. Fig. 4 shows $\dot{V}$ as a function of $\rho \in [0, \bar{\rho} = 10]$ and $\gamma \in [-\pi, \pi]$. Gains have been selected such that the surface $\dot{V}$ is negative across our region of interest.

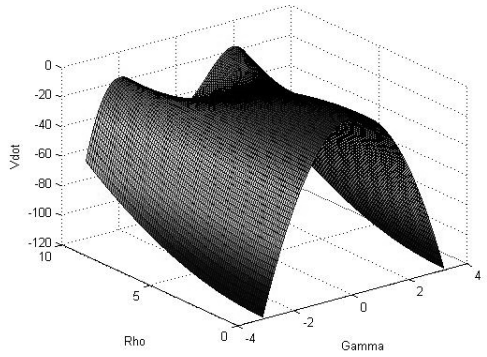

Fig. 4. Plot of surface $\dot{V}$, $k_\rho = 0.5$, $k_\gamma = 12$

IV. Controller Implementation

A. Single Goal Manipulation

In order to test the control strategy presented in Section III, the algorithm was implemented on the custom AFM setup outlined in Section II. As an initial test of the controller, the planned manipulation was simulated using MATLAB. Fig. 5 shows a plot of the manipulation of a single particle to a target point located at the origin (0,0).

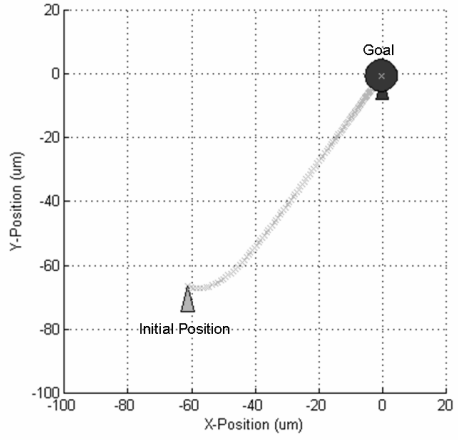

Fig. 5. Simulation of a single particle manipulation

As can been seen in simulated manipulation in Fig. 5, the action of the controller is to first reposition the tip behind the particle, correcting the error in γ. In the event that the particle begins to slip or slide about the tip, the orientation controller will correct this before the particle loses contact with the tip and manipulation must be restarted. The particle is then pushed along a straight line path to the goal position. The speed of manipulation is limited by the feedback rate of the camera and framegrabber. As noted earlier the update rate for the particle positions is only 10-15 Hz.

For the first set of experiments, a single particle is moved in line with a second reference particle. Fig. 6a shows the configuration of the particle at the start of the algorithm for one of the experimental trials. The first step in the manipulation algorithm is to detect all of the particles within the image plane using the gradient detection algorithm. In the next step, the user selects the particle to be manipulated, locates the AFM probe tip, and then defines the target position for the particle. To minimize the amount of computation during the gradient detection algorithm a "region of interest" is formed around the particle. Rather than search the entire image at each frame update, only this region is searched for the particle. After selecting the target position, particle is moved into contact with the tip. Once the tip comes into contact with the tip, the controller is turned on and run until the particle reaches the target position. The particle is released from the tip by lifting the slide in the z-direction and the tip is returned to its initial position. The final configuration of the particle is shown in Fig. 6b.

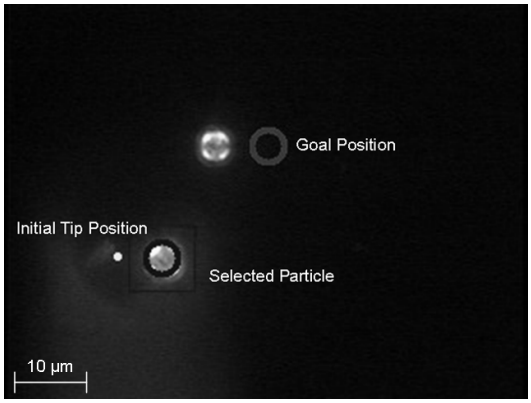

Fig. 6a. Single target point – before manipulation

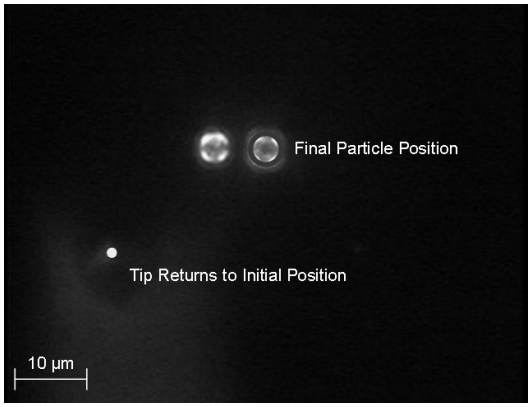

Fig. 6b. Single target point – after manipulation

This control strategy was repeated across several trials. Pushing to a single target point was achieved in a single manipulation without restarting and without loss of contact with the particle. To illustrate the corrective action of the controller when the particle begins to spin about the tip, refer to Fig. 7. Shown is the orientation control log for a trial

where particle begins to spin on the tip. Spinning occurs when the tip and particle are not aligned along the same trajectory.

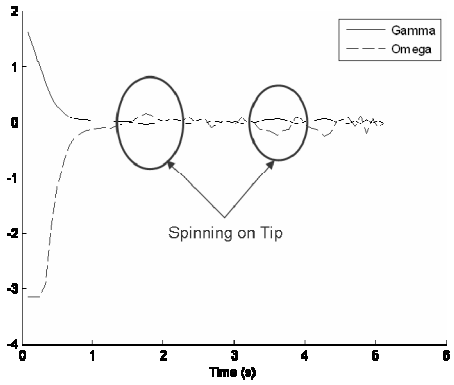

Fig. 7. Experimental control output log

As can be seen, the controller is able to correct the orientation of the particle with respect to the tip when it begins to spin around the tip. It should also be noted that the noise that can be seen in the controller log is due to the uncertainty in the gradient based detection algorithm. As the particle is manipulated, changes in illumination and reflection result in a 1-2 pixel (0.3-0.6 μm) uncertainty in the position of the particle. This often leads to actions that are unnecessary or over corrective. This is also problematic as the particle approaches the target position. Near the target, small changes in the particle position can result in large spikes in the orientation error.

B. Multi-Point Manipulation

Above, it was shown that autonomous manipulation of a particle to a single unobstructed target point could be achieved. However a more complicated problem is to manipulate the particle to an obstructed point by defining a series of goal points that takes the particle around any obstacle. In this second experiment the user defines a series of goal points that can be linked together by unobstructed paths to reach a final target point. Fig. 8a shows such a complex path to an obstructed target point.

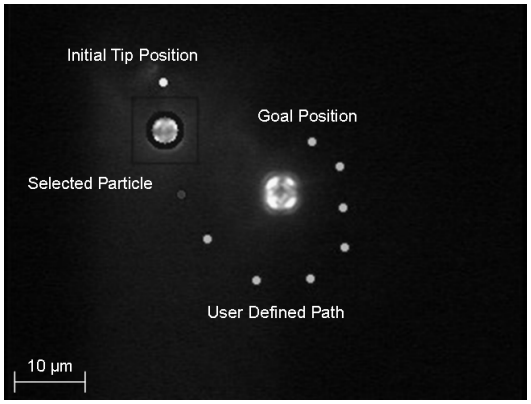

Fig. 8a. Muti-target path – before manipulation

For demonstration purposes this path is exaggerated such that it will not come into contact with another particle. It has already been established that convergence to a single point is guaranteed, therefore if a series of points are evaluated sequentially, convergence to the final point in the series is also guaranteed. The final configuration is shown in Fig. 8b.

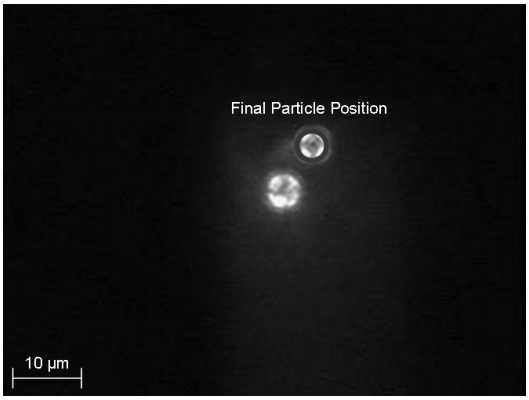

Fig. 8b. Muti-target path – after manipulation

C. Automatic Path Planning and Manipulation

In the previous section it was established that a complex trajectory to a target position can be defined by linking together a series of operator selected points. The next step is to develop a strategy to automatically identify obstructions in the particle's path and automatically define a safe path that will avoid collision with other particles. This is another scenario where techniques from the macro world can be applied to micromanipulation and nanomanipulation. Obstacle avoidance has been studied extensively for robotic applications [10]. As discussed earlier the particle has been effectively modeled as a non-holonomic wheeled vehicle. For this application, cell decomposition and implementation of the wavefront expansion or grassfire algorithm can effectively locate a navigable path [13].

The first step is to decompose the image frame into a 10 μm x 10 μm cell grid. Each cell is then checked to see if it is occupied by any part of one of the particle. Each occupied cell is labeled with an 'x.' Having located the cells that are occupied by neighboring particles, a path is located along free cells by implementing a wavefront expansion algorithm (Fig. 9).

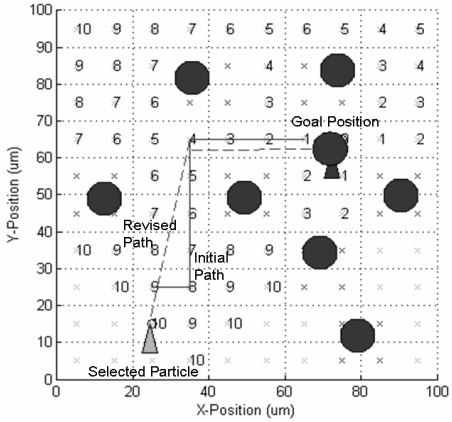

Fig. 9. Shortcut found along initial path

The goal cell is located and labeled with the number '0.' The algorithm then marks each adjacent, unoccupied cell with the number '1.' Each cell that has not been marked and

is unoccupied and adjacent to '1' is marked with a '2'. This process continues until the cell containing the selected particle is found. The number assigned to each cell corresponds to the number of steps from the goal. If the starting cell is not found then it is concluded that there is no unobstructed path to the specified goal cell. If a path to the goal exists, it can be found by starting at the selected particle and counting down to 0 while minimizing the Manhattan distance to the goal cell.

Though a path is found it is clear that this is not the most efficient way to reach the goal. To minimize the time needed to navigate to the goal, the path planning algorithm searches the path starting from the goal, checking each point to see if there is a shortcut between points. In this example a shortcut is located from start to 3 and then from 3 to the goal. Thus the 10 point path is reduced to a single intermediate point. The revised path is indicated by the dashed line in Fig. 9.

Adding this path planning algorithm to the previous manipulation program significantly increases its utility. Essentially an operator can select any particle in the image frame and move it to any target position for which a navigable path exists. To demonstrate this programs effectiveness, several trials were run in which a particle was required to be navigated through a field of obstacle particles to a desired target position (Figs. 10a and 10b)

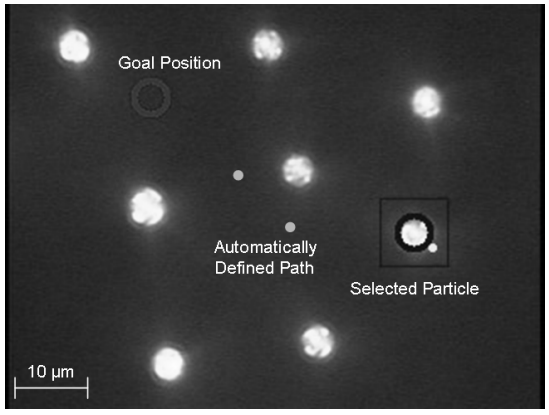

Fig. 10a. Automatic path planning – before manipulation

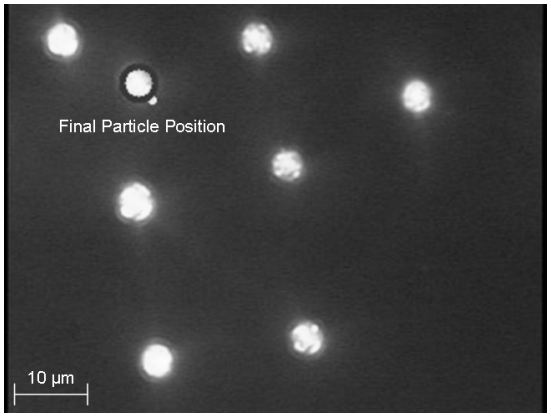

Fig. 10b. Automatic path planning – after manipulation

V. Conclusion

In this paper a strategy for controlled pushing of 4.5 µm PS particles has been presented. This controller utilizes visual feedback at 10-15 Hz to track particle positions and control the input velocity and direction of the tip. With this controller, particle positioning was achieved with a precision of less than 3 pixels (0.87 µm).

The primary focus of this paper has been manipulation at the microscale. However in order to extend the ideas of this paper to the nanoscale additional study is required to account for assumptions that have been neglected. These include tip deflections, particle deformation, and inertial forces. Future development will incorporate piezoresistive probes to provide force feedback to the controller. Additional study is also needed to develop a reliable particle release strategy. In the current approach, positioning accuracy is hindered due to difficulty in releasing the particle from the tip when the target has been reached.

References

[1] C. D. Onal and M. Sitti, "Visual Servoing Based Autonomous 2D Manipulation of Microparticles using a Nanoprobe," *IEEE Trans. on Contr. Syst. Technol.,* accepted, 2006.

[2] A. Tafazzoli, C. Pawashe, and M. Sitti, "Atomic Force Microscope based two-dimensional assembly of micro/nanoparticles," *Proc. of the 6th IEEE Int. Symp. on Assembly and Task Planning*, pp. 230-235, Montreal, Canada, July 2005.

[3] A. Menciassi, A. Eisinberg, I. Izzo, and P. Dario, "From "macro" to "micro" manipulation: models and experiments," *IEEE Trans. on Mechatronics*, Vol. 9-2, pp. 311–320, 2004.

[4] T. R. Ramachandran, C. Baur, A. Bugacov, A. Madhukar, B. E. Koel, A. Requicha, and C. Gazen, "Direct and controlled manipulation of nanometer-sized particles using the noncontact atomic force microscope," *Nanotechnology*, vol. 9, no. 3, pp. 237–245, Sept. 1998.

[5] C. Pawashe and M. Sitti "Two-Dimensional vision-based autonomous microparticle manipulation using a nanoprobe", *Journal of Micromechatronics*. vol. 3, nos. 3-4, pp. 285-306, 2006.

[6] Hansen, L. T., Kuhle, A., Sorensen, A. H., Bohr, J., and Lindelof, P. E., "A technique for positioning nanoparticles using an Atomic Force Microscope", *Nanotechnology*, vol. 9, pp. 337-342, 1998.

[7] A. Tafazzoli and M. Sitti, "Dynamic modes of nanoparticle motion during nanoprobe-based manipulation," *Proc. of the 4th IEEE Conference in Nanotechnology,*pp. 35-37, Munich, Germany, August 2004.

[8] A. A. Rad, K. Faez, and N. Qaragozlou, "Fast Circle Detection Using Gradient Pair Vectors," *Proc. VIIth Digital Image Computing: Techniques and Applications*, Sun C., Talbot H., Ourselin S. and Adriaansen T. (Eds.), 10-12 Dec. 2003.

[9] B., Bhushan, *Introduction to Tribology*. New York, NY: John Wiley & Sons, 2002.

[10] R. Siegwart and I. Nourbaksh, *Introduction to Autonomous Mobile Robots*. Cambridge, MA: Bradford. pp. 81-86, 284-285, 2004.

[11] A. Astolfi, "Exponential stabilization of a mobile robot." *Proc. of 3rd European Control Conf.*, pp. 3092-3097, Rome, Italy, September 1995.

[12] S.-O. Lee, Y.-J.Cho, M. Hwang-Bo, B.-J. You, R. Oh: "A Stable Target-Tracking Control for Unicycle Mobile Robots," *Proc. of the IEEE/RSJ Int. Conf. on Intelligent Robots and Systems*, pp. 255-267, Takamatsu, Japan, November, 2000.

[13] R. Jacobs and J. Canny, "Planning Smooth Paths for Mobile Robots," *Proc. of IEEE Conf. Robot Autom.,*, pp. 2-7, 1989.

[14] H.K. Khalil, Nonlinear Systems, 2nd Edition, Prentice Hall, 1996.